Batteries & Supercaps

Research Article
doi.org/10.1002/batt.202500559

Chemistry Europe
European Chemical Societies Publishing

www.batteries-supercaps.org

Analyzing the Impact of Electrolyte Motion Induced Salt Inhomogeneity Effect on Apparent Aging: Role of Current Rates and Temperature Effects in Accelerated Cyclic Aging Tests in Li-Ion Batteries

Pablo Morales Torricos,* Andreas Gallenberger, Dominik Droese, Julia Kowal, Christian Endisch, and Meinert Lewerenz

Accurate and rapid assessment of lithium-ion battery lifetime is essential for predicting remaining lifespan, enabling the selection of appropriate cells for specific applications and determining suitability for second-life use. However, accelerated cyclic aging tests may underestimate a cell's total lifespan due to exaggerated capacity fade that does not occur under real-world conditions. This increased capacity fade is primarily driven by electrolyte motion induced salt inhomogeneity (EMSI) and loss of homogeneity of lithium distribution (HLD). This study investigates the impact of varying charge and discharge currents on capacity loss during accelerated testing in compressed NMC-Gr pouch cells. Most of the capacity loss observed during cycling is fully recoverable after a resting period, with some cells regaining up to 81% of their lost capacity. Contrary to expectations, cells subjected to the highest cycling currents do not exhibit the greatest recoverable capacity loss. This phenomenon can be attributed to the interplay between current and temperature: While higher cycling currents exacerbate EMSI and HLD loss, they simultaneously elevate cell temperature, which mitigates EMSI by weakening polarization, enhancing electrolyte salt diffusion and homogenizing lithium distribution in the anode. Consequently, higher temperatures counteract HLD and EMSI-effect and therefore reduce apparent capacity loss.

1. Introduction

An accurate and rapid estimation of lithium-ion battery (LIB) lifetime is crucial for optimizing resource efficiency in both battery manufacturing and the application strategies of OEMs. Accelerating aging mechanisms during cyclic tests, such as applying high currents and eliminating resting phases, allows for faster estimation of cyclic battery performance compared to real life aging tests. However, these testing conditions have been shown to induce undesired effects, such as recoverable capacity loss[1–9] and, in some cases, recoverable resistance degradation.[5–7,10]

Previous investigations have linked the apparent aging to a loss of homogeneity of lithium distribution (HLD),[2,5,10] which refers to the uniformity of intercalated lithium in the anode. During continuous cycling, some areas of the anode become less lithiated than others, resulting in areas with lower potential. For this reason, during a discharge capacity test, the lower voltage limit is reached earlier, leading to apparent capacity loss. During a subsequent resting phase, lithium has time to redistribute across the anode, reducing the voltage differences between differently lithiated anode areas and finally leading to a higher measured capacity. Hence, apparent aging is a direct consequence of loss of HLD in the anode. Considering apparent aging is therefore crucial for an accurate lifetime prognosis during accelerated cyclic aging tests, as the reversible capacity loss is significantly larger (up to nine times) than theirreversible amount.[4,5]

A noninvasive measurement of HLD is possible through differential voltage analysis (DVA), by observing changes in the shape of the dV/dQ versus Q curves through the test. HLD loss is observable as a flattening of the anode features during cycling and a recovery of their shape during resting. This process occurs simultaneously with capacity loss and recovery, suggesting the previously mentioned correlation between HLD and apparent aging.

A possible mechanism causing loss of HLD is the electrolyte motion induced salt inhomogeneity (EMSI) effect, first proposed by Solchenbach et al.[6] EMSI effect is caused by electrolyte pumping, which occurs only when two conditions are met: mechanical confinement of the jelly roll and significant volume expansion of the graphite due to lithiation.[11–13] Loss of HLD has also only been observed in cells with mechanical compression (cylindrical cells,[5,10] prismatic,[1,2] and compressed pouch[4,14]), and its severity

P. Morales Torricos, A. Gallenberger, C. Endisch, M. Lewerenz
Research Group Electromobility and Learning Systems
Technische Hochschule Ingolstadt
Esplanade 10, 85049 Ingolstadt, Germany
E-mail: els@thi.de

D. Droese, J. Kowal
Chair for Electrical Energy Storage Technology (EET)
Technische Universität Berlin
Einsteinufer 11, 10587 Berlin, Germany

Supporting information for this article is available on the WWW under https://doi.org/10.1002/batt.202500559

increases with increasing stiffness of the confinement.[4] These findings suggest that EMSI is a plausible mechanism behind the loss of HLD, as both effects only appear under similar mechanical conditions. Furthermore, as EMSI reduces electrolyte conductivity at the jelly-roll edges, it is expected to influence lithiation rates across the cell, closely relating to the HLD loss.

Apparent aging is known to be favored during cycling with high charge currents[5,6,10] and continuous operation without rest periods.[1,2,14] Nevertheless, the independent influence of charge and discharge currents, as well as temperature, on EMSI and HLD has not yet been analyzed.

In this study, we investigate how current rates affect the EMSI effect and HLD loss in mechanically constrained pouch cells. The compression, ambient temperature, depth of discharge (DOD), and average state of charge (SOC) are selected to induce EMSI. The influence of current rates is investigated by reducing the maximum charge current while keeping the discharge current constant and vice versa. Since changes in current rate also affect test duration and resistive heat generation, temperature plays a crucial role for this investigation. Finally, we review the latest findings on apparent aging caused by EMSI and HLD loss and extend the EMSI/HLD model to deepen the understanding of accelerated cyclic aging tests.

2. Results and Discussion

This section presents the evolution of capacity, resistance, and DVA for cells compressed to 321 kPa along with an explanation of these results based on the interplay between temperature, EMSI, and HLD. Corresponding results for the capacity and HLD of the cells compressed to 642 kPa are provided in the Supporting Information.

2.1. Influence of Temperature and Current Rates on EMSI Effect and HLD during Cycling

The influence of temperature and current rates on the EMSI effect and the loss of HLD is not yet fully understood. This chapter provides a review of the current state of research on the formation and evolution of EMSI in compressed Li-ion pouch cells based on the work of Solchenbach et al.[6] Zimmermann et al.,[13] Schreiber et al.,[10] Bond et al.,[11] and Morales Torricos et al.[4] It also examines how EMSI can be influenced by charge and discharge currents, as well as by a temperature increase resulting from resistive heat generation. In addition, we summarize previous findings related to apparent aging and HLD based on the work of Lewerenz et al.[2] and Morales Torricos et al.,[5] demonstrating how DVA can assess lithium distribution homogeneity within the anode. Finally, we present a possible pathway through which salt gradients can lead to the loss of HLD in the anode.

Figure 1 illustrates the EMSI and HLD generation processes during an accelerated cyclic aging test with a cycling window of 100% DOD. The through-plane salt concentration gradient caused by charge and discharge is shown in the first row (a–d), EMSI generation in the second row (e–h), HLD development in the third row (i–p), and the interplay of EMSI and HLD in the fourth row (q-t). Despite these effects occurring simultaneously, they are presented separately for clarity. Figure 1 demonstrates the impact of mechanical constraint on the jelly-roll using a schematic of a single cell layer (anode–separator–cathode) during a cyclic aging test. EMSI is absent under uncompressed conditions (a–d) but is triggered under compression (e–h). Furthermore, to illustrate loss of HLD in the anode, graphs (i–p) present an assessment of HLD loss with DVA published by Morales Torricos et al.[5] and Lewerenz et al.,[1,2] along with a graphical depiction of a cell with generated EMSI and HLD loss (q–t). This model is based on findings by Solchenbach et al.[6] (EMSI), Schreiber et al.[10] (EMSI and HLD), Lewerenz et al.[2] (HLD), and Morales Torricos et al.[4,5] (HLD and pressure).

The cycling procedure for an uncompressed lithium-ion cell is illustrated in Figure 1a–d, where the cell is neither constrained by an external mechanism nor enclosed in a rigid housing. In a pristine cell (a), the concentration of $LiPF_6$ is homogeneous in the cell stack, shown by a yellow color of the electrolyte. During charging (b), a through-plane salt gradient is formed, with a lower $LiPF_6$ concentration near the anode current collector and a higher concentration near the cathode current collector. Simultaneously, lithium-ion intercalation causes the graphite anode material to expand, leading to an increase in anode particle and cell volume, depicted by the red arrows. During discharge (c), the cell undergoes polarization in the opposite direction, resulting in a high salt concentration near the anode current collector and a low concentration near the cathode current collector. Furthermore, the NMC cathode also undergoes volume expansion during discharge, but this expansion is negligible compared with that of the graphite anode, as reported by Spingler.[15] After cycling (d), the salt gradient within the cell rapidly rehomogenizes, as only a through-plane gradient on a micrometer scale was present.

The effect of the same cycling procedure on a compressed cell is shown Figure 1e–h. As in the uncompressed case, the pristine cell (e) initially exhibits a homogeneous distribution of $LiPF_6$ in the electrolyte. During charging (f), the same through-plane salt gradient develops; however, the restricted expansion of the now compressed cell leads to two key effects: a reduction in anode porosity and the compression of the soft separator.[16,17] Both effects decrease the overall cell porosity, causing displacement of electrolyte out of the jelly-roll (white arrows). The displaced electrolyte is retained within the pouch bag most likely in the anode overhang region. The precise location depends on the cell format (cylindric, prismatic, or pouch) and the cells orientation during cycling, as reported by various authors.[6,11–13] Due to the salt gradient formed during charging, the electrolyte displaced from the anode has on average a lower $LiPF_6$ concentration. During discharge (g), the shrinking graphite particles increase both anode and separator pore volume, drawing the previously displaced, low-concentration electrolyte back into the anode, leading to a salt depletion at the electrode edges. With repeated and continuous charge–discharge cycles, this effect becomes increasingly pronounced. After the cycling phase (h), the cell exhibits a significant in-plane salt gradient, with a low

Research Article
doi.org/10.1002/batt.202500559

Chemistry Europe
European Chemical Societies Publishing

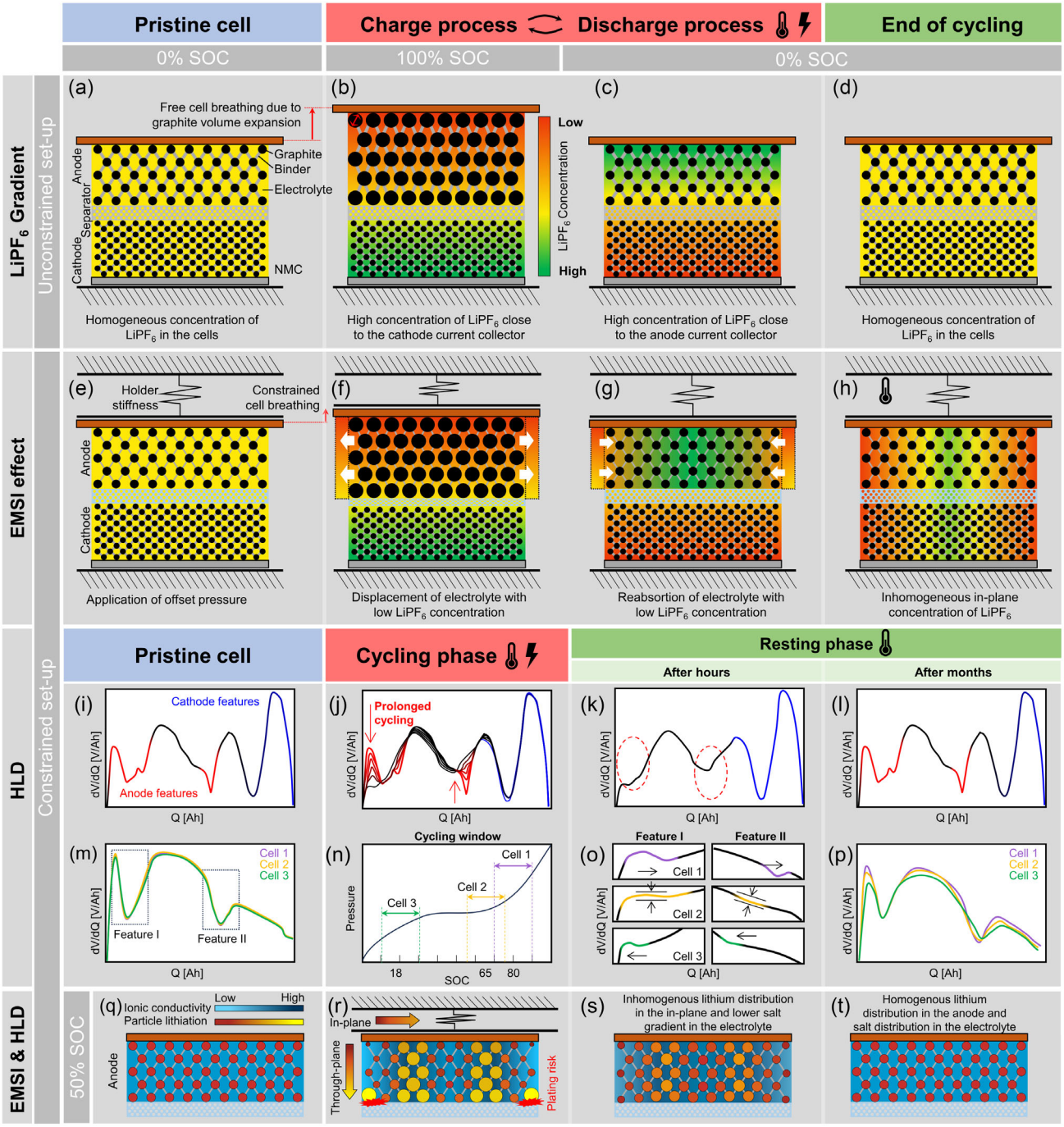

Figure 1. Interplay of $LiPF_6$ gradient, EMSI, and HLD generation in a compressed and uncompressed setup during cell cycling. a–d) $LiPF_6$ gradient during charge and discharge in an uncompressed setup. e–h) EMSI generation in a cell under compression. i–l) Loss of HLD in the anode and cathode features (sketched from Morales Torricos et al.[5]). m–p) Differences in peak flattening behavior of the characteristic anode features depending on different cycling conditions (sketched from Lewerenz et al.[2]). q–t) Schematic for a possible interplay between EMSI generation and HLD loss. The process steps during cycling influenced by cycling current and temperature are highlighted with a current and temperature icon (b), (c), (h), (j), (n), and (r).

salt concentration in the electrolyte at the electrode edges and a high salt concentration at the cell's center, both in the anode and the cathode. This salt gradient results in areas with different conductivities in the in-plane direction, as both low and excessively high concentrations of $LiPF_6$ reduce electrolyte conductivity.[18,19] Moreover, a higher holder stiffness was also correlated with a greater amount of apparent aging.[4] This is a key point in understanding the interplay between EMSI, apparent aging, and HLD.

A summary of findings regarding apparent aging and HLD is presented in Figure 1i–p. This relationship has been documented in previous studies[2,4,5,10] via correlation of capacity measurements with the non-invasive method of DVA. Figure 1i shows

the d*V*/d*Q* vs *Q* curve of a NCA/Gr + Si cell in a pristine state with the anode features marked in red and cathode features in blue (sketched from Morales Torricos et al.[5]). In this pristine state, the entire cell is expected to have a homogeneous lithium distribution. During continuous cycling with high current rates, the graphite features progressively flatten until they become nearly indistinct, as illustrated by the color transition from red to black in Figure 1j. The flattening of these features indicates a loss of HLD in the anode during cycling, a phenomenon not observed for the cathode, as seen in the blue sections of the d*V*/d*Q* versus *Q* curves. Even after a few hours of resting post-cycling, the anode features remain absent, as highlighted by the red ellipses in Figure 1k. After an extended resting period (weeks to months) at a low SOC, the anode features fully reappear, as illustrated in Figure 1l. The extended duration required for rehomogenization, which is similar to the recovery time of the anode overhang effect,[10,20] suggests that lithium diffuses over relatively long distances between anode regions with different lithiation levels, rather than just between neighboring particles, which would result in a much faster recovery. In addition to the shape restoration of the d*V*/d*Q* vs *Q* curve, the measured cell capacity also returns to its initial value, indicating a reversible aging mechanism associated with lithium redistribution in the anode. Consequently, the observed flattening is not attributed to irreversible aging processes such as lithium plating or SEI formation, but to an inhomogeneous lithium distribution in the anode.

The d*V*/d*Q* versus *Q* curves change shape differently depending on the cycling conditions, as reported by Lewerenz et al.[2] In this context, Figure 1m–p show the DVA for three compressed NMC(1:1:1)/Gr cells subjected to accelerated cyclic aging tests with different cycling windows. The initial d*V*/d*Q* vs *Q* curves for the three cells, each cycled at a different average SOC, are shown in Figure 1m, with the anode features highlighted within two boxes. Figure 1n shows the cycling window of the different cells (*x*-axis) and the corresponding experienced pressure change (*y*-axis), demonstrating that all cells experienced significant volume changes during cycling, which are necessary to generate EMSI. After prolonged cycling, the anode features of the different cells exhibited different changes in the shapes of features I and II, as demonstrated in Figure 1o, emphasizing the diversity of inhomogeneous lithiation patterns that can develop in the anode. For example, the features of Cell 1 shift to the right, those of Cell 2 remain stationary but flatten, while Cell 3's features shift to the left. Furthermore, the different inhomogenization patterns are fully reversible during the resting phase (Figure 1m,p), where all three cells recover toward their original shape. Since the capacity loss and subsequent recovery correlate with these changes in the d*V*/d*Q* versus *Q* curves, the evolution of curve shape during DVA offers a non-invasive method to infer the actual lithium distribution in the anode.

To date, the precise mechanism by which EMSI leads to a loss of HLD is unclear. A correlation between the two phenomena is evident, as both are associated with apparent aging in capacity and, in the case of silicon-containing cells, with resistance. Further, both effects occur during prolonged cyclic aging with high currents, particularly when the large lithiation-induced volume changes of the anode particles are constrained by a stiff jelly-roll confinement (e.g., rigid housing or externally compressed pouch cells). Therefore, we hypothesize that EMSI induces in-plane salt concentration gradients, which result in a non-uniform charging of the anode during cycling. This imbalance gradually gives rise to inhomogeneous lithium distribution within the anode. Although this process is not yet fully understood, we present a possible pathway by which EMSI may lead to the loss of HLD, based on previous investigations.

Figure 1q–t shows a possible pathway by which EMSI could lead to a loss in HLD over the anode. For this purpose, the anode of a single-layer cell at 50%SOC is illustrated, with the graphite particles' lithiation levels depicted from lower (dark brown) to higher (gold) than 50%SOC. The electrolyte ionic conductivity is represented from low (light blue) to high (dark blue), depending on the salt concentration.[6,11] The lithiation states and electrolyte conductivity are presented for four conditions: pristine (q), during cycling (r), shortly after cycling (s), and after an extended resting period (t).

The pristine cell state is shown in Figure 1q, where both the lithiation degree of the graphite particles and the conductivity of the electrolyte are homogeneously distributed. Figure 1r illustrates a possible lithium distribution within the anode and a corresponding conductivity gradient in the electrolyte during cycling. The figure represents a potential cell state at the end of a charge to 50% SOC during cycling, where electrolyte regions with low or excessively high salt concentrations exhibit reduced conductivity (light blue), while areas with moderate salt levels and therefore higher conductivity appear in dark blue.[21]

After prolonged cycling, the in-plane salt gradient resulting from EMSI (depicted by the color transition from dark to light blue) leads to an uneven in-plane charge distribution (illustrated by the variation in particle colors and the horizontal arrow). Particles in regions with higher ionic conductivity (dark blue) charge more rapidly than those in regions with lower conductivity (light blue). This is reflected in the particle colors: Lighter tones indicate higher lithiation, while darker tones indicate lower lithiation in the in-plane direction.

In the through-plane direction, particles near the separator show a higher degree of lithiation compared with those near the current collector due to slower lithium transport in low conductivity regions. This through-plane inhomogeneity is depicted by the vertical arrow on the left side of Figure 1r and is more accentuated in regions with low conductivity.

Moreover, EMSI affects not only the distribution of lithium but also contributes to irreversible aging effects. Decreased conductivity at the electrode edges increases the risk of lithium plating, due to either hindered lithium transport in the through-plane direction or a drop in anode voltage below 0 V versus Li/Li$^+$, as reported by Solchenbach et al.[6]

Figure 1s shows the cell after a resting period of several hours, when through-plane processes have concluded, such as lithium redistribution between neighboring particles.[22] In contrast, in-plane lithiation gradients within the anode persist, as large areas remain differently lithiated due to the long diffusion paths on the centimeter scale.[23] This is consistent with the slow rates of DVA

Research Article
doi.org/10.1002/batt.202500559
Chemistry Europe
European Chemical Societies Publishing

and capacity recovery reported in literature.[2,4–6,10] At this stage, both lithium and salt rehomogenization occur simultaneously. For the electrolyte, we assume partial rehomogenization of salt concentration, indicated by a reduced blue gradient in the anode, although, to our knowledge, the recovery rate of salt inhomogeneities has not yet been studied.

After a resting phase of several weeks or months the conductivity gradient and inhomogeneous in-plane lithiation are fully rehomogenized (Figure 1t) leading to a recovery of the apparent capacity loss and a reappearance of the characteristic peaks in DVA.

After discussing the given EMSI and HLD model, we introduce our understanding of the influence of current rates and temperature. The corresponding process steps in Figure 1 are highlighted with current and temperature icons. Higher current rates lead to a stronger through-plane salt gradient during polarization (b, c),[24] and with this, a higher salt gradient in in-plane direction after prolonged cycling (h).[22,24] At the same time, a stronger in-plane salt gradient induces increased salt diffusion, which promotes rehomogenization. This counteracting effect intensifies with the gradient, suggesting that beyond a certain current threshold, further salt inhomogenization is limited, hinting at a saturation of the effect of increasing current rates on the generation of EMSI.

Processes affected by an increasing cell temperature include the weakening of through-plane salt gradient during polarization (b, c),[25] the accelerated in-plane redistribution of salt (h),[26] and redistribution of lithium within the anode in the in- and through-plane direction due to a faster ionic transport by migration and diffusion (r, s).[21]

As current rates increase, resistive heat generation causes an additional rise in internal cell temperature. This leads to two opposing effects on EMSI: While higher currents promote EMSI due to stronger polarization, the resulting temperature increases, and concentration gradient enhances ionic transport and support the rehomogenization of salt distribution. Therefore, current rate and temperature have counteracting effects in EMSI formation. This study contributes to a better understanding of their interplay during accelerated cyclic aging tests.

2.2. Apparent Capacity Loss

The capacity loss and recovery of all cells at 321 kPa is presented in **Figure 2**. Cells at the maximum charge current of 2 A are shown in the top graphs, with colors ranging from yellow to magenta representing increasing absolute discharge currents from −1.13 to −3.4 A. Similarly, the bottom graph shows cells subjected to the maximum discharge current of −3.4 A with colors from cyan to magenta indicating rising charge currents from 0.67 to 2 A. The capacity loss during the cycling phase (Figure 2a) is plotted against full cycle

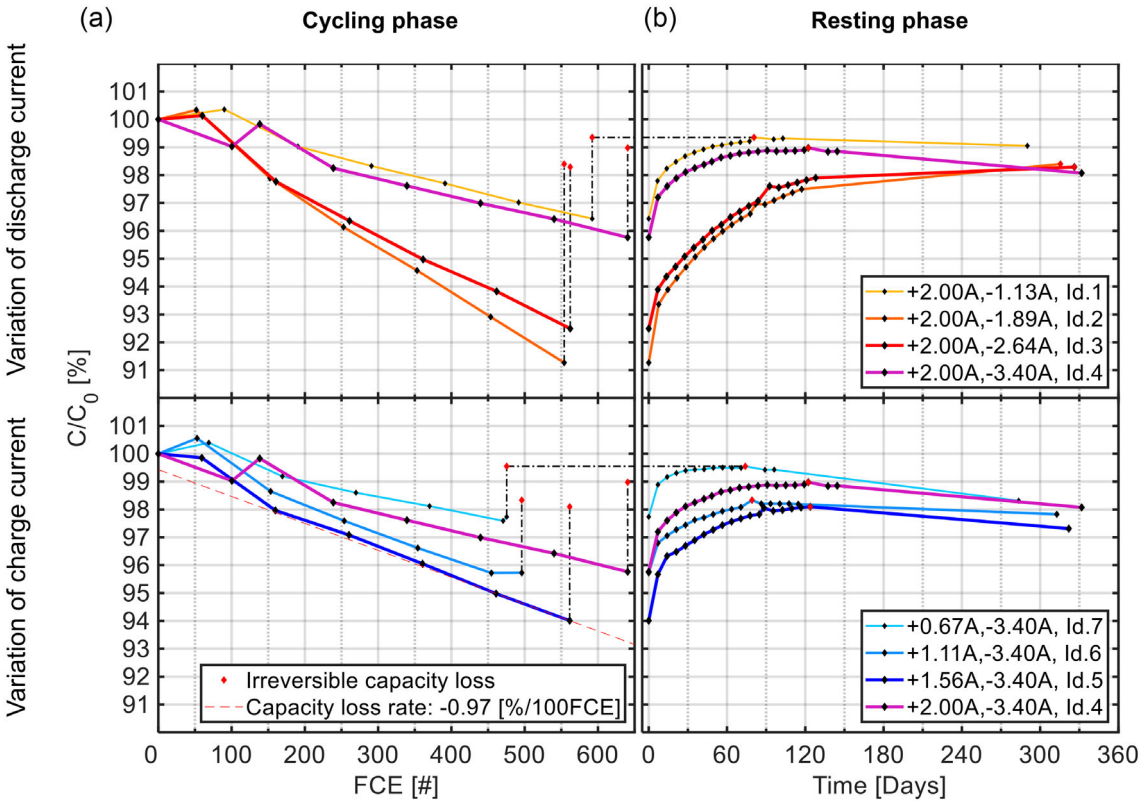

Figure 2. a) Capacity loss during the cycling and b) capacity recovery during resting for pouch cells cycled with different charge and discharge current rates and compressed to 321 kPa. The cycling and resting phases, as well as checkups, were carried out in a temperature chamber set to 25 °C, except for the final 6 months of rest, during which the cells were stored at 10 °C. The capacities of the cells were measured during each check-up with C/3 discharge. The method for calculating the capacity loss rate is depicted exemplary for Cell 5, with its capacity loss rate given in the legend. In (b), the irreversible capacity loss for each cell is presented with a diamond mark with red edge, which corresponds to the highest capacity value during resting.

equivalents (FCE), while the capacity recovery during the resting phase is plotted against the resting time (Figure 2b), facilitating the identification capacity loss and recovery rates.

The last checkup during the cycling phase of cells 6 and 7 shows an increasing trend (450–500 FCE). This occurred due to an unintended stop during the cycling phase between the sixth and seventh checkups, which led to a cell rest of 30 (Cell 6) and 6 h (Cell 7). This short rest period was sufficient to slightly reverse the capacity loss from the previous cycles, which is acceptable since the resting period was started after the next check-up.

Capacity loss and recovery vary strongly between cells, indicating that capacity trends are heavily influenced by the applied cycling currents. During the cycling phase, applying the highest charge and discharge currents does not lead to the highest capacity losses, as seen in Figure 2a. Specifically, the cells at the extremes of the current ranges, those with the lowest discharge current (yellow), the lowest charge current (cyan), and the highest charge and discharge currents (magenta), exhibit the lowest capacity loss rates, while cells operating at intermediate current levels experience higher capacity loss rates.

During a resting phase at 10% SOC (Figure 2b), all cells exhibit significant capacity recovery. At low SOC, the steep slope of the anode voltage curve results in large voltage differences between anode particles with varying lithium content, which in turn accelerates the rehomogenization of lithium within the anode. The cells were stored at 25 °C for the initial 4 months to accelerate capacity recovery and then simultaneously transferred to 10 °C for the following 8 months to minimize calendric aging. Most cells reach their maximum capacity recovery (diamond marker with red edge) within the first 4 months, after which they begin to lose capacity due to calendar aging—except for Cell 2 (orange) and Cell 3 (red), which continued to recover capacity throughout the subsequent 8 months.

The time required to reach maximum capacity recovery varies among the cells. For example, the cell with the lowest charge current (cyan) reaches the maximum of its recovered capacity earlier than the others. Interestingly, the cell subjected to the highest current rates (magenta) shows a similar recovery profile to Cell 1 (yellow), despite experiencing significantly higher discharge currents. This observation further indicates the distinct roles of charge and discharge currents in influencing EMSI, HLD, and capacity loss.

Previous studies have attributed capacity recovery to the rehomogenization of lithium distribution in the anode, as well as to the anode overhang effect.[4,5,10] In the present results, the latter is expected to contribute equally across all cells, as it depends solely on the difference between the average SOC during cycling and the resting SOC, which is identical for all cells. In a prior study using the same cells and compression set-up,[4] the anode overhang effect was estimated to account for ≈1% of the recovered capacity. This was observed in a cell with no pressure change, i.e., no EMSI generation during cycling. Therefore, the anode overhang effect alone cannot account for the total amount of capacity recovered in this experiment.

To estimate the irreversible capacity loss due to cycling, the maximum recovered capacity during rest (diamond marker with red edge) is used as a reference. This value is tracked both during the resting and cycling phases to assess the true impact of cycling at different current rates on cell aging. The results indicate that a significant portion of the capacity loss during cycling is reversible, which has important implications for aging prognosis under varying current conditions.

However, a direct comparison of cycling-induced capacity loss is challenging due to the varying number of cycles completed in each test, as cells with higher current rates cycle faster than those with lower currents. To address this the apparent aging of the cells will be further evaluated by examining the capacity loss rate (expressed in [%/100 FCE]) instead of the total lost capacity.

2.3. Pulse Resistance

The internal resistance of the cells during cycling and resting phases is shown in **Figure 3**a,b. The measurements are taken at the end of each checkup using a 3.4 A charge pulse at 50% SOC after 10 s. These cells have an average initial resistance of 64.6 ± 1.0 mΩ. Only Cell 6 has a significantly larger initial resistance of 83.4 mΩ due to a bad electrical connection during the first checkup. Nevertheless, its resistance throughout the remainder of the study follows the general trend and exhibits similar absolute values to those of the other cells. Therefore, the second checkup value is used to calculate the relative resistance increase of Cell 6.

The resistance increase during the cycling phase (Figure 3a) is minimal for all cells. Cells 1–4, which were cycled at the maximum charge currents, show a maximum resistance increase of 7%, while Cells 4–7, cycled at maximum discharge currents, exhibit a maximum increase of only 3%.

There is no clear correlation between resistance increase and capacity loss. Among Cells 1–4, Cells 2 and 3 exhibit the highest capacity loss rates, along with only slightly higher resistance increases. However, this trend does not persist during the resting phase, as all resistance values increase with similar rates. For Cells 4–7, no clear correlation is observed, as resistance increases remain uniformly low. Notably, unlike capacity, resistance does not return to its initial value (100%) during rest in all cases. Therefore, in contrast to previous studies on cells with Si–Gr anodes,[4,5,10,27] the observed capacity recovery in this case cannot be explained by a recovery of cell resistance.

Figure 4 presents the resistance evolution of the cells compressed to 642 kPa during the cycling (a) and resting (b) phases. As with the 321 kPa group, the resistance increases steadily throughout both phases, with no observable recovery during rest.

Over the entire test period, resistance increases up to ≈15% for most cells, except for Cell 14, which shows a slightly higher increase of around 20%. These results are in good agreement with those from the 321 kPa set, confirming the reproducibility of resistance and capacity trends across both test conditions.

Importantly, the resistance increase during the cycling phase (Figure 4a) is minimal—typically under 5%—making its contribution to resistive heat generation negligible. These findings highlight the stability of internal resistance during cycling and reinforce the conclusion that resistive heat generation is primarily governed by current rate rather than resistance changes.

Research Article
doi.org/10.1002/batt.202500559
Chemistry Europe
European Chemical Societies Publishing

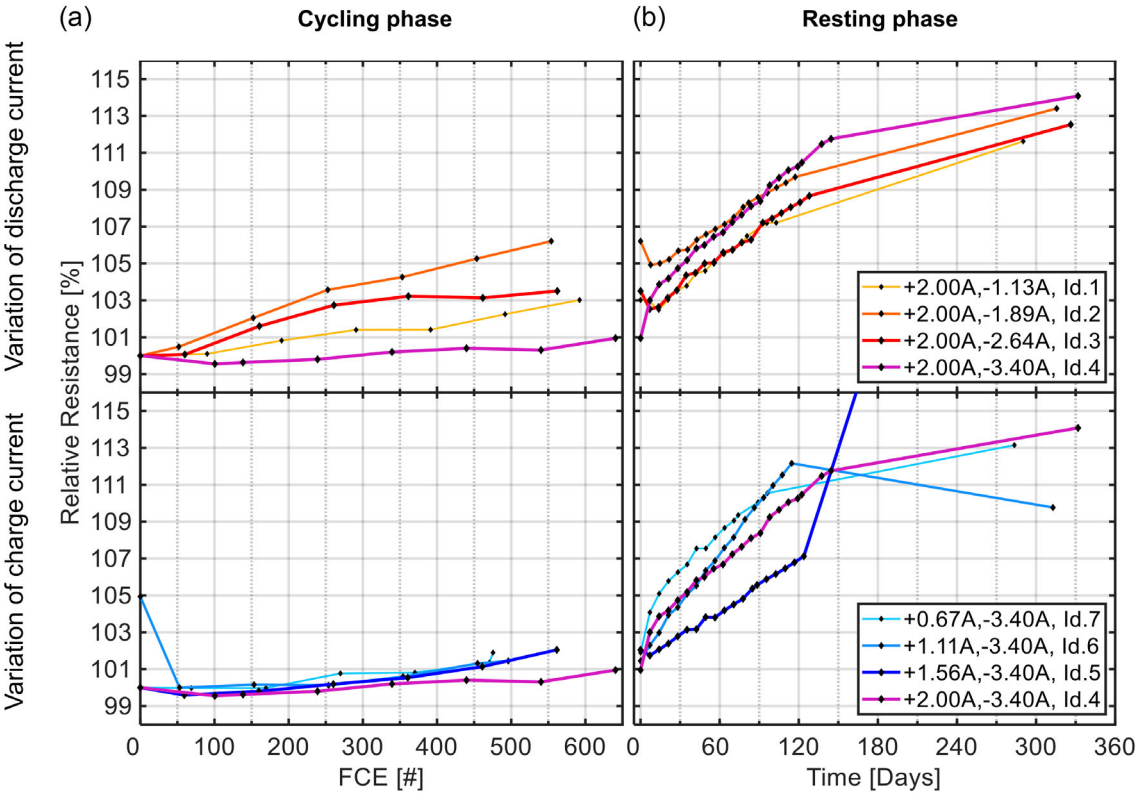

Figure 3. Pulse resistance at 50% SOC with a charge pulse of 3.4 A after 10 s during a) cycling and b) resting phases for pouch cells compressed to 321 kPa and cycled with different charge and discharge rates.

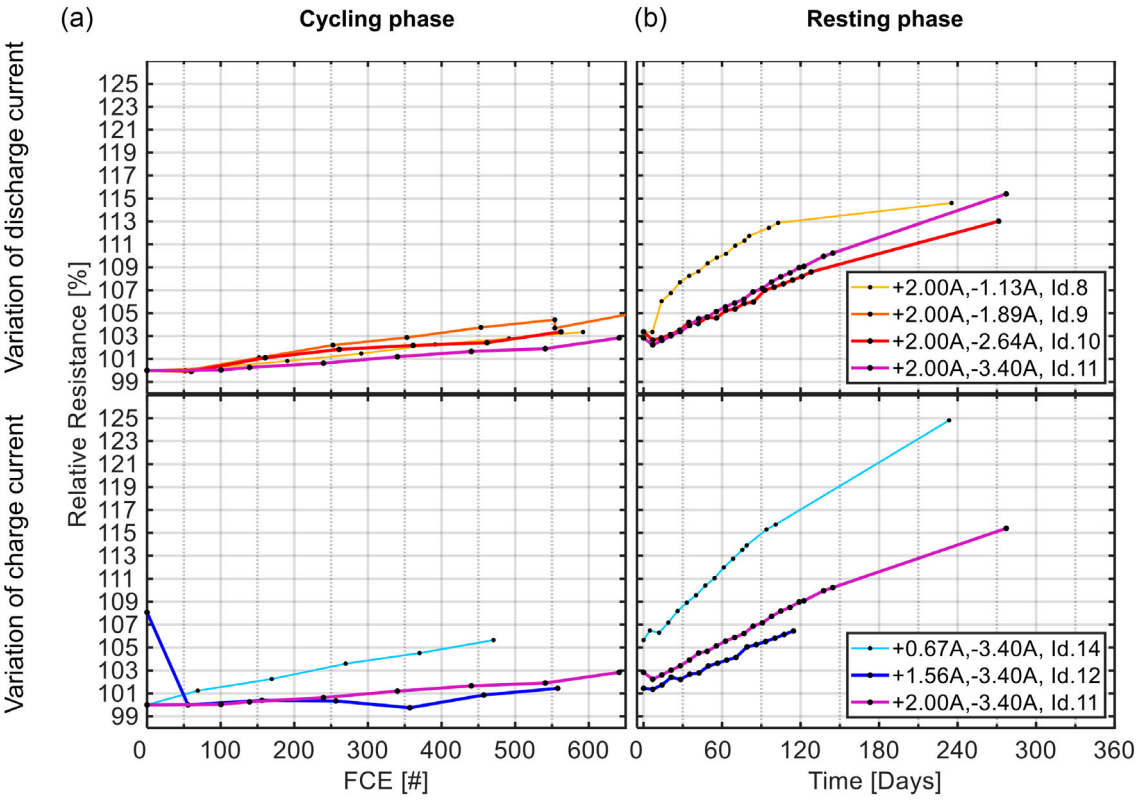

Figure 4. Pulse resistance at 50% SOC with a charge pulse of 3.4 A after 10 s during a) cycling and b) resting phases for pouch cells compressed to 642 kPa and cycled with different charge and discharge rates.

Note that the resistance data for Cell 13 during the resting phase, and the final checkup value for Cell 12, are missing. Cell 13 was excluded from the resistance plot due to significant noise caused by poor electrical contact with the battery cycler. Nonetheless, based on consistent trends across the remaining cells, a similar resistance evolution is expected for Cells 12 and 13.

2.4. Inhomogeneity of Lithium Distribution

To assess the occurrence of EMSI and HLD in this study, we apply DVA and focus on the anode features in the d*V*/d*Q* vs. *Q* curves. **Figure 5** illustrates the shape transformation of the d*V*/d*Q* vs. *Q* curves during cycling (a) and resting (b) phases for one exemplary cell (Cell 6). In Figure 5a, the cell in its pristine state is represented by the black dashed curve (0 FCE), while the cell after cycling is shown in red (497 FCE). In Figure 5b, the cell status immediately after cycling is represented by the red curve (0 weeks), while the red-to-green transition curves correspond to the resting phase, with green color representing the 13th resting week. The blue curve represents the state of the cells after around 1 year of resting.

The evolution of the curve shape reveals the level of inhomogenization on the cell's anode. We observe the phase transitions from Stage IV to Stage III and from Stage II to I in the graphite anode (between 0.2–0.5 and 2–2.5 Ah), hereafter referred to as Peak I and Peak II. A flattening of these features indicates a more inhomogeneous lithium distribution within the anode, as different electrode areas pass asynchronously between the phases at different lithiation degrees, causing the anode feature in the d*V*/d*Q* versus *Q* curve to flatten. The anode features, which flattened during cycling, recover during the resting phase, and the peak (marked with a black dot in the zoomed plot) moves toward its initial position, showing a gradual increase in HLD across the anode. It is important to note that changes in the shape of the DVA curve provide insight only into the HLD of the anode, and not into the distribution of lithium within the electrolyte. Consequently, all references to HLD in this publication pertain exclusively to the homogeneity of lithium distribution within the anode. A detailed analysis of the shape change of all d*V*/d*Q* vs *Q* curves for all cells is offered in the Supporting Information in section "HLD during cycling and resting."

The peak height is computed as the maximum value between 0.1 and 0.4 Ah during the CC charge with C/15. This metric for assessing the homogeneity of lithium distribution is chosen, as Peak I fully recovers during the tests. However, considering the entire curve shape evolution during DVA may provide a more comprehensive quantification of HLD and EMSI within the cell. This use of DVA may allow the identification of the different recovery sources and their corresponding rates, allowing even a non-invasive quantification of apparent capacity loss during cycling. Nevertheless, this is beyond the scope of this investigation.

By plotting the peak height of Peak I for the different cells during both the cycling and resting phases, the degree of inhomogenization and its dependence on current rate can be determined throughout the test. This is shown in **Figure 6**, where the peak height is plotted over the cycling and resting phases for each cell at 321 kPa. The top graphs present cells with the same charge current of 2 A, while the bottom graphs show the cells with the same discharge current of −3.4 A.

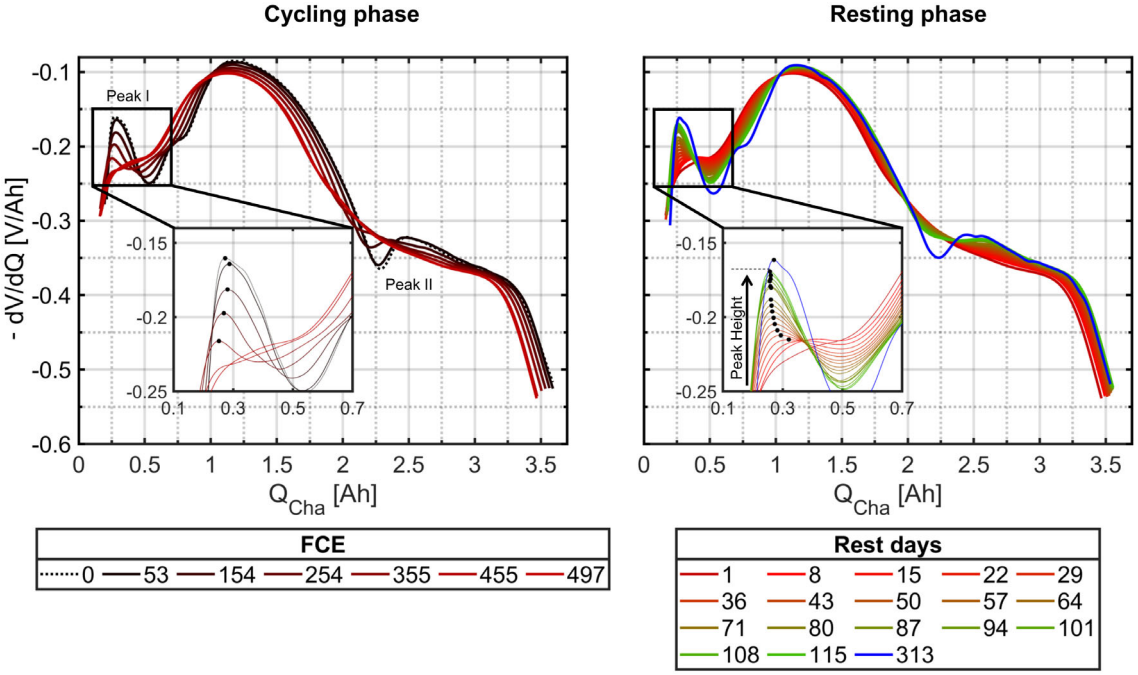

Figure 5. Evolution of the d*V*/d*Q* vs. *Q* curves for Cell 6 during the cycling and resting phases, along with the stage transitions of graphite (Peaks I and II). During cycling, the curve evolves from the pristine cell state (dashed line) to the highest cycled state after 497 cycles (red line). During the resting phase, the curve evolves from the first resting day (red) to 115 days of rest (green), and up to 1 year of rest (blue line). The height of Peak I (black dot) is calculated as the maximum value in the zoomed-in window (0.1–0.4 Ah) and becomes indistinguishable after 455 FCE.

Research Article
doi.org/10.1002/batt.202500559
Chemistry Europe
European Chemical Societies Publishing

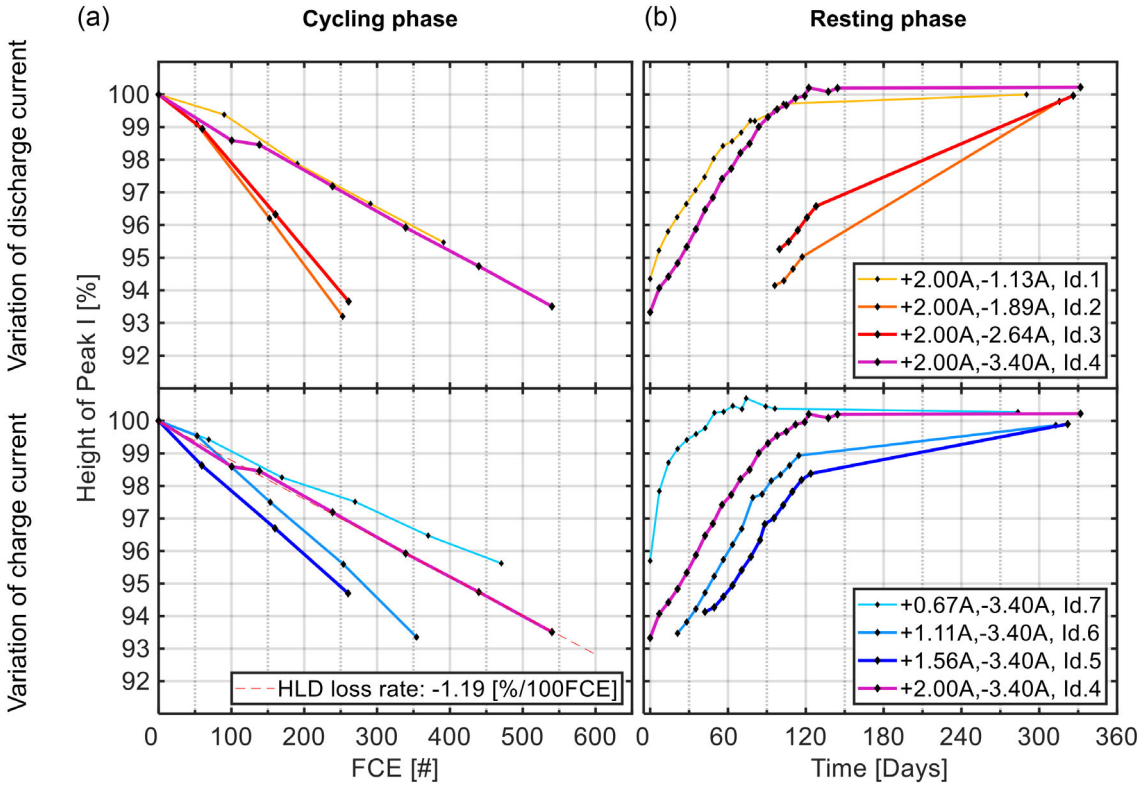

Figure 6. The loss and recovery of HLD are assessed through the height of peak I during the a) cycling and b) resting phases for pouch cells compressed to 321 kPa and cycled at different current rates. Only distinguishable peaks in the d*V*/d*Q* versus *Q* curves are considered, leading to gaps after a certain cycle when the peak height becomes unidentifiable. The HLD loss rate is shown exemplary for Cell 4 with a dashed red line.

Some curves in Figure 6 appear to be incomplete, as not for all checkups, the peak height is measurable. This is the case because after extended cycling, the anode features flatten to a point where the peak height becomes indistinguishable. This occurs for cells with very pronounced inhomogeneity of lithium distribution.

The evolution of the d*V*/d*Q* versus *Q* curves for all cells during the cycling and resting phases is shown in the Supporting Information: **Figure 7** for cells compressed to 321 kPa and **Figure 8** for those compressed to 642 kPa.

In Figure 6a (cycling phase), the highest degree of inhomogenization does not correspond to the highest current rates, as would be expected considering only the influence of current rate on EMSI. Notably, the order of the curves in the capacity and HLD plots during cycling is identical: The slowest degradation occurs in cells cycled at lower current rates (Cells 1 and 7), followed by a peak in degradation at intermediate currents (Cells 3 and 5), and a reduction in degradation at the highest currents (Cell 4).

In Figure 6b (resting phase), the height of Peak I returns toward its initial value (100%) for all cells over the entire rest period. This means that all cells are fully recovered and the state-of-charge distribution throughout the anode area is expected to be highly homogeneous. Thus, the capacity loss from EMSI and HLD is expected to be completely recovered. In some cases, the peak height slightly exceeds 100% at the final checkup (e.g., Cells 1, 4, and 7). This minor increase is due to the accuracy of the peak height identification method, which relies on a fitting algorithm that is susceptible to small changes in chamber temperature. Additionally, the anode overhang effect can slightly alter the DVA shape.[28]

In summary, the loss of HLD during cycling shows a strong correlation with changes in capacity. Nevertheless, the recovery rate varies among the cells. In the following section, we compare the loss rates of capacity and HLD by analyzing the gradients of the curves shown in Figure 2 and 6.

2.5. Influence of Current Rates and Offset Pressure on Apparent Aging

In this section, we examine the impact of cycling currents and offset pressure on capacity loss, HLD, temperature and recovery time, as shown in Figure 7a–d. The results summarize these aging metrics during cycling (a, b, and d) and resting (c) for 14 cells. Diamond markers represent cells compressed to 321 kPa, while circular markers indicate cells compressed to 642 kPa. The *x*- and *y*-axes correspond to the charge and discharge currents applied during cycling.

The capacity loss rate is not the highest in the cells cycled at the highest currents as shown in Figure 7a. Increasing the charge current leads to more apparent capacity loss up to 1.56 A. Increasing the discharge current causes a similar effect up to

Research Article
doi.org/10.1002/batt.202500559
Chemistry Europe
European Chemical Societies Publishing

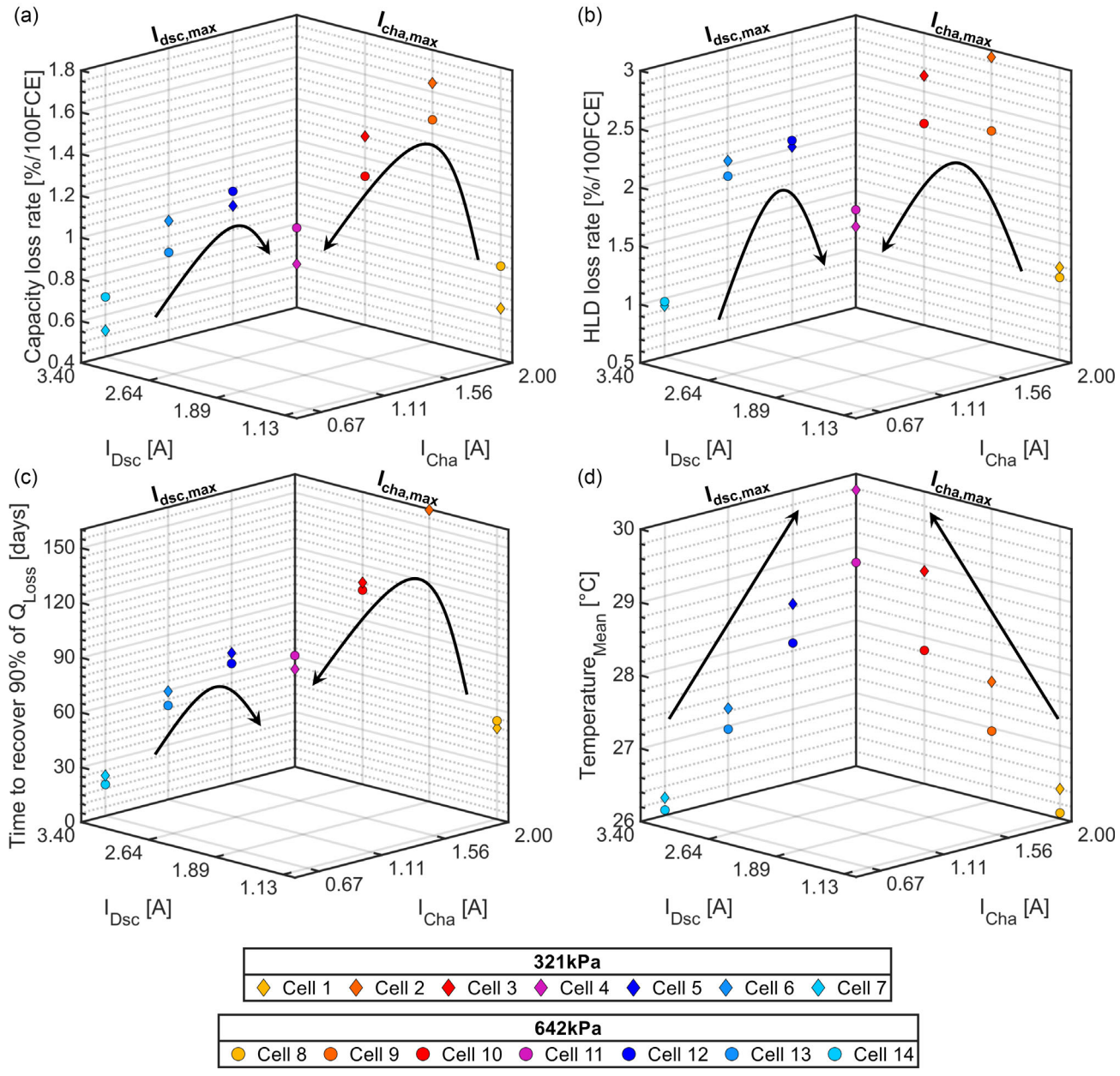

Figure 7. a) Capacity loss rate, b) inhomogeneity of lithium distribution (HLD loss rate), c) time to regain 90% of the total capacity recovery, and d) average temperature during cycling for all cells. Data is shown for cells compressed to 321 kPa (diamonds) and 642 kPa (circles), cycled under varying charge and discharge currents.

1.89 A. Beyond these points, the capacity loss rate starts to decline with increasing currents. Ultimately, the cells cycled at the maximum current rates (magenta) show capacity loss rates similarly low to those of cells cycled at the lowest charge or discharge currents. The non-monotonic increase suggests a significant influence of temperature on apparent aging, which will be discussed in a later paragraph.

The HLD loss rates (Figure 7b) follow the same trend as the capacity loss rates (Figure 7a). HLD loss rates increase with rising charge and discharge currents up to a certain threshold, beyond which the loss rate begins to decrease. As a result, Cells 4 and 11 (magenta), which were cycled at the highest current rates, show HLD loss rates comparable to those cells with either the minimum charge current (cyan) or discharge current (yellow). This strong correlation suggests that, in this particular test, capacity loss is primarily driven by the loss of HLD. Consequently, changes in the characteristic peaks of the DVA curves serve as a reliable indicator for estimating apparent aging in cyclically aged cells affected by the EMSI effect.

The aforementioned dependency between apparent aging and HLD is further supported by analyzing the time to recover the capacity and HLD losses during the resting phase. Figure 7c shows the time to regain 90% of the total capacity recovery. The recovery time of Cell 9 is not shown in this graph

Research Article
doi.org/10.1002/batt.202500559
Chemistry Europe
European Chemical Societies Publishing

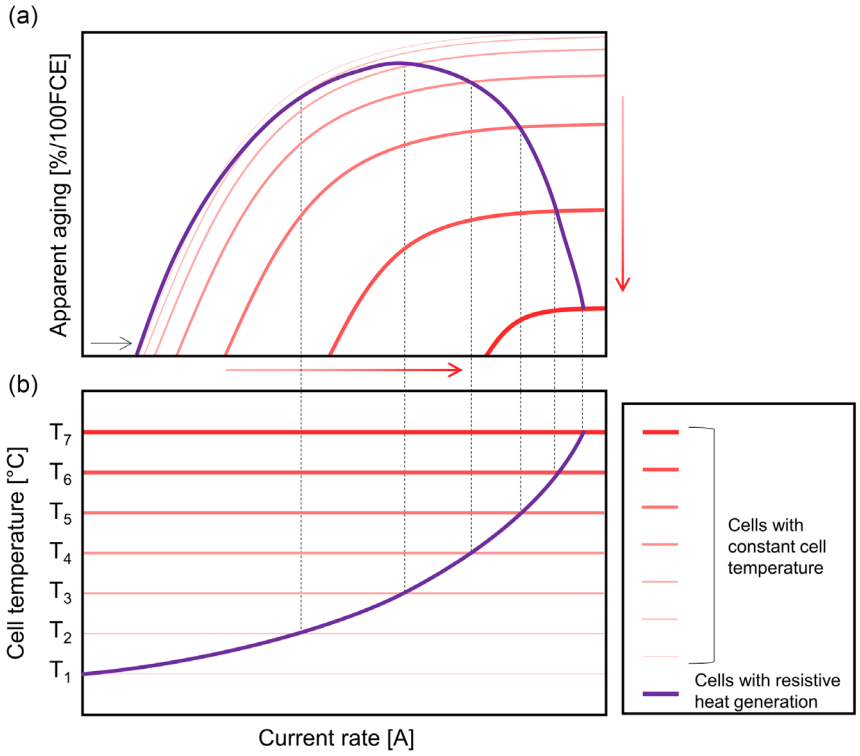

Figure 8. Sketch of the influence of temperature on apparent capacity loss. In a), the apparent aging is sketched for a given temperature profile in b). Red curves are constant temperature scenarios, assuming no resistive heat contribution. The purple curve includes resistive heat at the ambient temperature T_1.

as it underwent further cycling for additional testing. The recovery times of all other cells follow the same trend previously observed for capacity and HLD loss rates, indicating that cells with higher inhomogenization also require more time to rehomogenize. Only marginal differences were observed in the recovery times of cells compressed at 321 and 642 kPa, suggesting that the offset pressure does not significantly influence lithium rehomogenization processes in the anode. The slight variations in recovery time between the different compression levels are therefore likely attributable to cell-to-cell variations. Furthermore, the consistent trend in capacity and HLD loss rates observed across both offset pressures indicates a high reproducibility of the results.

During cycling, the cells experienced different temperatures depending on the magnitude of the applied current rates and offset pressures. To more accurately measure the temperature caused by resistive heat generation, an additional test was carried out using two pristine cells. In this test, the temperature at the negative tab was measured during cycling across all current rates and both pressure conditions. The detailed test description and temperature profiles for all current rates and a corresponding summary are provided in the Supporting Information (Figure 3 and 4). Cells cycled at 321 kPa consistently exhibit higher mean temperatures during cycling than those cycled at 642 kPa, as shown in Figure 7d. One possible explanation is the better heat conduction to the compression plates at higher pressures that would slightly decrease the temperature. For both cases, the mean temperature shows an almost linear increase with higher currents as the influence of the quadratic resistive heat is weakened by reduction of the internal resistance with increasing temperature. Although this temperature measurement does not account for additional heating from resistance growth due to aging, it remains strongly representative, as the resistance increase observed for all cells during the test is negligible (see Figure 3a).

For a direct comparison of the impact of increasing charge and discharge currents, it is important to note that the magnitude of the charge currents in this test is significantly lower than that of the discharge currents. Despite this, cells cycled with maximum charge currents generally show higher capacity loss rates than those cycled with maximum discharge currents as seen in Figure 7a. The origin of this behavior is discussed in more detail in the following section.

3. Discussion

We attribute the observed apparent aging primarily to the loss of HLD in the anode. This conclusion is supported by the strong correlation between apparent capacity loss and the shape evolution of the dV/dQ versus Q curves during cycling and resting. Specifically, as capacity decreases during cycling, the peak height of graphite Feature I also diminishes. During resting, both recover at a similar rate, indicating their strong relationship. Hence, HLD loss in the anode is the main contributor to apparent aging, as motivated bythe following observations: 1) A strong correlation is

observed between capacity loss and the flattening of characteristic anode features in DVA. Both capacity and HLD decrease during cycling but are largely recovered during a subsequent resting period. 2) The DVA shows no changes in the cathode features[5] during cycling or resting, motivating that the inhomogeneity of lithium distribution mostly occurs in the anode and not the cathode. 3) The loss and recovery of capacity cannot be attributed to changes in resistance, as resistance increases monotonically throughout the test without showing any signs of recovery. Resistance recovery has so far been observed only in silicon–graphite composite anodes,[5,6,10] but not in pure graphite anodes.[4] Thus, salt inhomogeneity does not affect pulse resistance, making DCIR a better indicator for state-of-health (SOH) estimation for these cells. 4) Even at low resting SOCs, the recovery of capacity and HLD takes weeks or even months, which is similar to the rehomogenization duration of the anode overhang effect,[29] hinting at large distances between differently lithiated anode areas.

However, EMSI is the underlying mechanism for the loss of HLD. The in-plane salt gradient leads to uneven charge distribution during cycling, which, under prolonged cycling, generates HLD loss over the anode. This is strongly supported by the absence of apparent aging in tests where electrolyte is not displaced during cycling, due to a lack of a rigid housing (cells compressed with low stiffen in ref. [4]), or the absence of lithiation-induced volume changes in the anode (cells with cycling windows with no graphite expansion in ref. [5,30]).

Our proposed mechanism on how cycling current rates and cell temperature influence apparent aging is presented in Figure 8. We first consider a scenario in which cells are cycled at a constant temperature neglecting resistive heat (e.g., direct liquid cooling). These cells are represented by red lines in Figure 8b, with lighter red curves indicating lower temperatures.

Figure 8a shows the expected apparent aging that the cells experience when cycling at different current rates, analogous to the capacity loss in Figure 7a. At low current rates, there is no apparent aging. This is because low cycling currents lead to a weak in-plane salt gradient, which has sufficient time to rehomogenize during cycling due to the long cycle durations (analogous to a pause during cycling). With higher current rates a stronger in-plane salt gradient is generated, which amplifies the loss of HLD and thus exacerbates apparent aging. The current rate threshold for the onset apparent aging is shown in Figure 8a by the black arrow on the *x*-axis.

Apparent aging saturates after a certain current rate, as very high salt concentration gradients enhance salt diffusion, counteracting further inhomogeneity. Increasing cell temperatures from T_1 to T_7 leads to a right shift of the onset threshold of the apparent aging curve toward higher currents, due to faster electrolyte diffusion rates at higher temperatures. Moreover, the maximum achievable apparent aging decreases for the same reason as indicated by the red arrows in Figure 8a. Notably, in a real-world scenario, the internal temperature of a cell depends not only on the ambient temperature but also on resistive heating and the thermal interface to its surroundings, such as cooling plates, compression pads, and other components.

Now, we assume an experiment including resistive heat generation starting at T_1 and ending at T_7, indicated by the purple curve. The resistive heat is increasing quadratically but weakens due to lower internal resistance of the cell toward higher temperatures following the measurement in Figure 7d. The corresponding apparent aging curve must fit the constant temperature curves at the given C-rates. The resulting purple curve in Figure 8a explains the behavior observed in Figure 7a and highlights that temperature plays a crucial role in how EMSI leads to a loss of HLD and apparent aging. Notably, we did not mention the influence of temperature on HLD recovery as we consider it to be comparably slow. This theory is consistent with many publications that observed lower capacity losses at higher cycling current rates.[31–33]

In the following, the individual influence of charge and discharge currents on EMSI formation leading to HLD loss and apparent aging is discussed. Higher charge currents induce stronger through-plane polarization, displacing electrolyte with lower salt concentration out of the jelly-roll. Upon reabsorption during discharge, this results in a pronounced in-plane salt gradient, with significantly reduced salt concentration and therefore electrolyte conductivity near the electrode edges. In contrast, higher discharge currents primarily lead to salt accumulation in the cell center, slightly reducing conductivity there. This behavior could explain the, on average, higher capacity loss rates for cells cycled at maximum charge currents compared to those cycled at maximum discharge currents, despite the significantly higher magnitudes of applied discharge currents, as seen in Figure 7a. As the trends observed in Figure 7a are similar for increasing charge and discharge currents, both must contribute to EMSI, HLD loss, and apparent aging. Thereby, higher cycling current rates increase the generation of EMSI through increasing polarization and shorter timespans for rehomogenization due to shorter cycle durations but also increase internal cell temperature through resistive heat generation, ultimately leading to a reduction in salt gradients through faster rehomogenization processes.

4. Conclusion

This study investigated the influence of charge and discharge current rates on the apparent aging of lithium-ion batteries. For this, apparent aging was induced by generating EMSI during cycling through the application of stiff mechanical cell compression. Fourteen compressed NMC-graphite pouch cells were cycled between 60% and 80% SOC in a temperature chamber set at 25 °C. To differentiate apparent from irreversible aging, the test protocol included a prolonged cycling phase (≈500 FCE), followed by a resting period of over 1 year. The cells were periodically assessed using checkup routines for capacity, DVA, and pulse resistance measurements.

Most of the capacity loss observed during cycling is attributed to recoverable effects, as over 81% of the initial loss was regained during the resting phase for all cells. In parallel, the HLD (assessed via changes in anode features from DVA) also decreased during cycling and recovered during resting, underlining the strong

Research Article
doi.org/10.1002/batt.202500559
Chemistry Europe
European Chemical Societies Publishing

correlation between HLD loss and apparent aging. In contrast, internal resistance increased steadily without any recovery. This decoupling supports the conclusion that apparent aging is primarily driven by the temporary loss of HLD rather than reversible changes in internal resistance.

Regarding current intensity, cells cycled at the highest current rates did not exhibit the greatest capacity loss. Instead, both capacity and HLD loss increased with increasing currents up to a certain threshold, beyond which further increases in current resulted in reduced apparent aging. This trend was consistent for both charge and discharge currents and was reproducible across all cells, independent of the applied offset pressure (321 kPa (7 cells) and 642 kPa (7 cells)).

We attribute this behavior to the combined influence of current and temperature on the EMSI effect. Higher currents increase through-plane salt gradients, which over prolonged cycling leads to stronger in-plane salt gradients and, consequently, to a higher loss of HLD and more pronounced apparent aging. Conversely, higher cell temperatures (arising from resistive heating at high currents) accelerate electrolyte diffusion processes and concentration gradients in the anode, thereby mitigating apparent aging. Thus, high current rates trigger two opposing effects: one that promotes and one that reduces apparent aging. The observed trend is therefore the result of these counteracting mechanisms, underlining the critical role of temperature in apparent aging.

Throughout this study, we identified several phenomena that remain insufficiently understood but are critical to deepening our understanding of apparent aging during cycling. These include: 1) The mechanisms governing the rehomogenization of salt gradients in the electrolyte and lithium distribution inhomogeneity in anode particles; 2) further variables influencing the in- and rehomogenization of lithium distribution in the anode, such as temperature, cell format regarding jelly-roll (wound, stacked, or z-stacked), cell housing, and module design; 3) the exact process by which EMSI leads to the loss of HLD in the anode; 4) the reason for the stability of cathode features in the dV/dQ vs Q curves, despite evident anode changes; and 5) the underlying cause of resistance recovery observed in silicon-containing anodes.

Additionally, we advocate for the non-invasive quantification of apparent aging through DVA analysis as a tool to improve lifetime estimation of lithium-ion batteries. Future accelerated aging tests must account for the EMSI effect and its contribution to lithium plating and, as shown in this investigation, apparent aging. This requires careful consideration and reporting of factors such as anode overhang, cell orientation, average SOC during cycling and rest phases, and resistive heat generation. Consequently, every accelerated aging protocol should include a resting phase to distinguish between reversible (apparent) and irreversible aging mechanisms.

5. Experimental Section

Fourteen pouch lithium-ion cells are compressed and aged through accelerated cyclic tests. Their technical specifications are detailed in **Table 1**. The cells are cycled using two battery testers by Arbin Instruments: LBTa2030 for eight cells (Cells 2, 3, 5, 6, 9, 12, and 13) and LBT21084 for the remaining six cells (Cells 1, 4, 7, 8, 11, and 14). The tests are conducted in temperature chambers by Binder (Model KB 115), set to a constant temperature of 25 °C. According to the manufacturer, these chambers have a spatial temperature variation of $\pm$0.2 K and a temporal temperature fluctuation of $\pm$0.3 K. Each cell is compressed with an apparatus that allows force monitoring. The force measurements are performed using C9C load cells from Hottinger Brüel and Kjaer, which have a nominal force of 10 kN with a reproducibility and repeatability error of less than 0.2%. The temperature is measured using a PT100 thermocouple on the negative cell tab, with data recorded through the auxiliary channels of the corresponding cyclers. The thermocouple is clamped onto the cell tab and shielded using thermally conductive, electrically insulating tape to ensure accurate readings without electrical interference.

Table 1. Technical data of the tested cell Model 103962-Lifun obtained from the official data sheet.

Producer	Lifun
Cell type	Pouch with wound jelly-roll
Cathode	NMC532
Anode	Graphite
Separator	PE + Mixed Coating
Electrolyte	EC + EMC + DMC + $LiPF_6$
Nom. capacity at 0.2 C	3.48 Ah
Max. discharge voltage	3 V
Nominal voltage	3.8 V
Max. charge voltage	4.35 V
Max. discharge current	3.4 A
Max. charge current	2 A
Weight	50 g
Length and height of the jelly-roll	55, 10 mm
Total cell width, width of contact area	38, 28 mm
Contact area	1556 mm^2

The apparatus shown in **Figure 9**a is designed to apply precise offset pressure to the cells. Each pouch cell is clamped between square aluminum plates (length, 85 mm, thickness, 12 mm) with M5 screws. The rigidity of the used plates and screws ensures that the volumetric change within the cell results in a mechanical stress perpendicular to the electrodes (in the through-plane direction). In this manner, the confinement of the jelly-roll ensures electrolyte displacement during cycling (in the in-plane direction), as the lithiation-induced volume change of graphite must compress the separator, anode and cathode. A force sensor located beneath the assembly monitors the force exerted perpendicular to the cell's largest surface.

The procedure for the compression of the cells is depicted in Figure 9b. To ensure an even pressure distribution across the cells during clamping, the torque is applied to the four screws in a cross-pattern, with the starting screw varied daily, as shown in the bottom graph in Figure 9b. After compression, viscoelastic stress relaxation causes the force to decrease over time. To reach and maintain the target force, the bolts are retightened after 24, 48, 72, and 96 h, as shown in the top graph. Testing begins once the force stabilizes within 5% of the target value over 24 h.

The cells are connected to battery cyclers using clamps, with each cell tab having three contact points for charge and discharge currents and an additional contact dedicated for monitoring, as illustrated in Figure 9c. The cell temperature is measured using electrically insulated thermocouples (PT100) positioned at the negative cell.

Research Article
doi.org/10.1002/batt.202500559
Chemistry Europe
European Chemical Societies Publishing

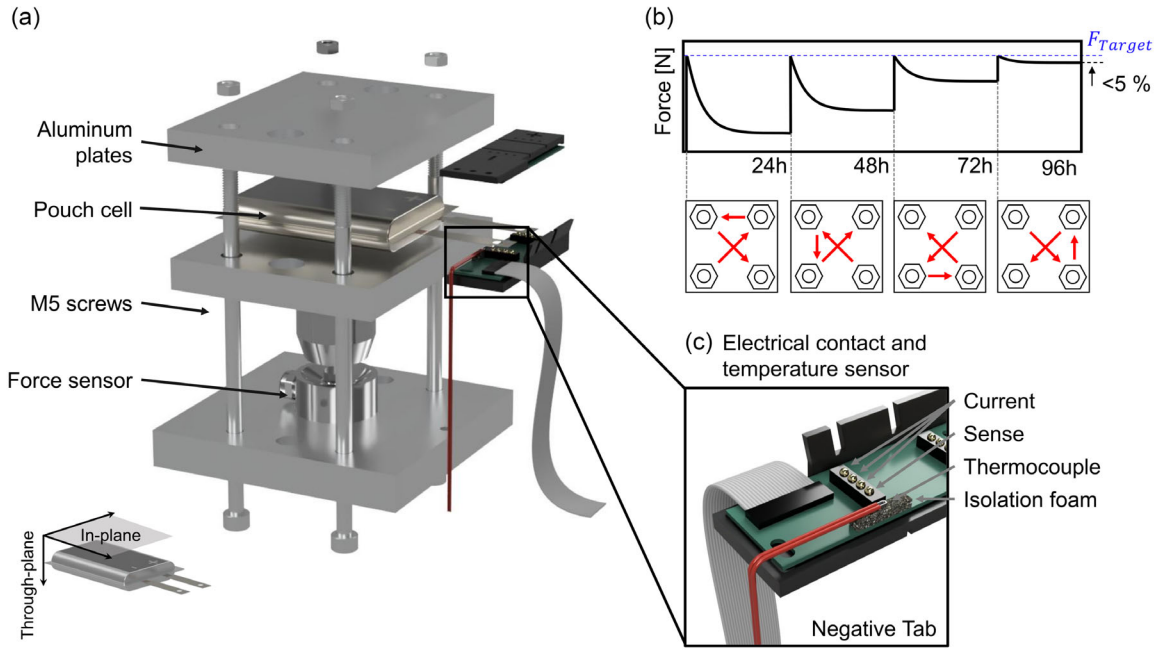

Figure 9. a) Apparatus for the compression of lithium-ion pouch cells with force measurement sensor and electrical connection. b) Compression procedure using the apparatus along with the corresponding force evolution. c) Detailed display of the electrical connection and temperature measurement on negative cell tab.

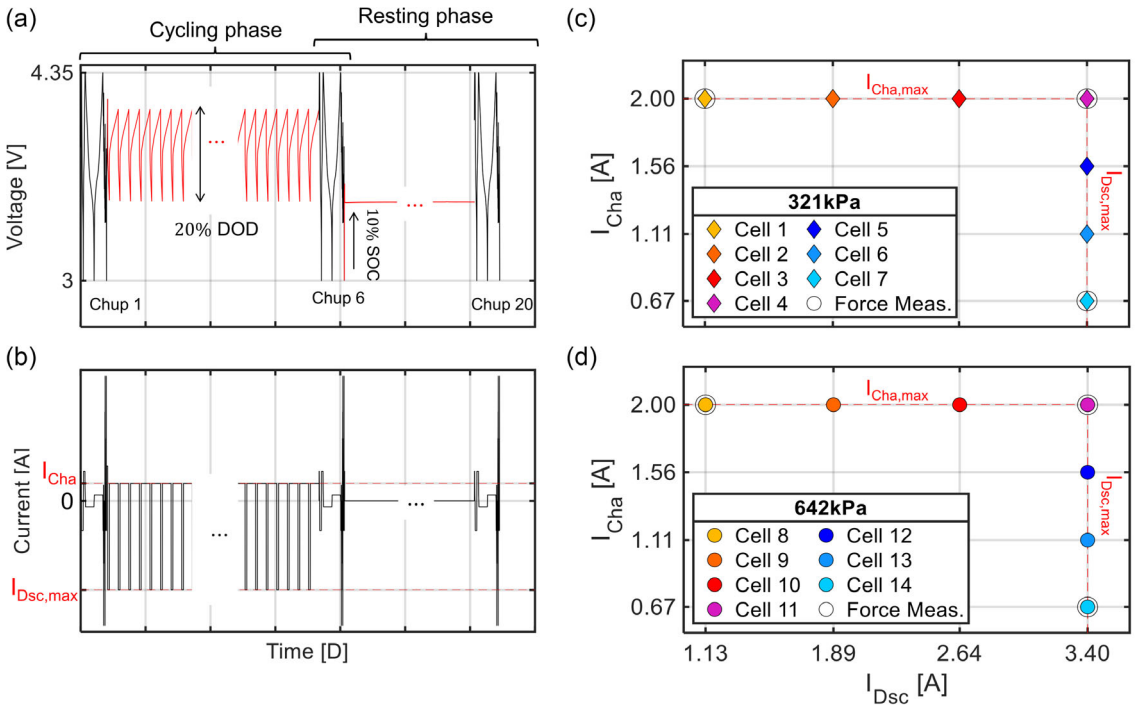

Figure 10. a) Strategy for the accelerated cyclic aging test consisting of a cycling and a consecutive resting phase. b) Charge and discharge currents during cycling applied during the test. c) Test matrix for cells compressed to 321 kPa. d) Test matrix for cells compressed to 642 kPa.

The test strategy consists of a cycling phase followed by a resting phase, as illustrated in **Figure 10**a. Throughout both phases, the SOH of the cells is assessed via a checkup routine conducted every 100 FCE during cycling. The cell voltage during cycling and resting phases is shown in red in Figure 10a, while checkup periods are marked in black. Figure 10b illustrates the cycling process with constant charge and discharge currents at a DOD of 20%, around an average SOC of 70%. This promotes the EMSI effect, driven by significant lithiation-induced volume changes in graphite.[4,5,34] The thickness change of a single graphite layer has been reported to be around ≈2.2%, which is

Table 2. Used sensors, pressures, charge and discharge currents for cell 1–14.

Cell Id.	Charge current [A]	Charge current rate [−]	Discharge current [A]	Charge current rate [−]	Pressure [kPa]	Pressure sensor
1	2.00	0.59	1.13	0.33	321	Yes
2	2.00	0.59	1.89	0.56	321	No
3	2.00	0.59	2.64	0.78	321	No
4	2.00	0.59	3.40	1	321	Yes
5	1.56	0.46	3.40	1	321	No
6	1.11	0.33	3.40	1	321	No
7	0.67	0.2	3.40	1	321	Yes
8	2.00	0.59	1.13	0.33	642	Yes
9	2.00	0.59	1.89	0.56	642	No
10	2.00	0.59	2.64	0.78	642	No
11	2.00	0.59	3.40	1	642	Yes
12	1.56	0.46	3.40	1	642	No
13	1.11	0.33	3.40	1	642	No
14	0.67	0.2	3.40	1	642	Yes

much larger than that of an NMC cathode (≈0.3%) within the same cycling window, based on measurements from Spingler et al.[15] The horizontal red dashed lines in (b) illustrate the cycling process with constant charge and discharge currents. During the resting phase, the cells are kept idle at 10% SOC. The temperature is 25 °C for the first 4 months, with checkups conducted every 5 days. For the remaining 8 months, the temperature is lowered to 10 °C, with one checkup conducted after ≈1 year of resting. The temperatures were selected to accelerate capacity recovery effects during the first resting months and reduce calendar aging for the rest of the resting months.

The tested cells are grouped into two sets of seven, as illustrated in Figure 10c,d, with only one cell per test condition. Cells 1–7 (diamond markers) are compressed with a clamping force of 500 N (321 kPa), while Cells 8–14 (circle markers) are subjected to 1000 N (642 kPa). The offset pressures are selected basing on,[4] since apparent aging is observed in compressed cells using these values at maximum current rates. Cells 1, 4, 7 and 8, 11, 14 are equipped with force sensors to accurately measure their force response over the duration of the experiment (presented with a black circle surrounding the markers). These measurements are used as a measure of EMSI generation during cycling, as discussed in the Supporting Information in Figure 2.

The cells without a force sensor (Cell IDs: 2, 3, 5, 6, 9, 10, 12, and 13) are compressed using a torque screwdriver of the brand Wera model 05074770001 (accuracy: ±6%) set to 16 and 32.5 N cm for the target forces of 500 and 1000 N, respectively. The applied force is verified using a force sensor, as discussed in more detail in the Supporting Information (Figure 1).

The checkup routine includes internal resistance measurements via pulse tests at 10%, 50%, and 90% SOC. At each SOC level, three consecutive charge pulses are applied with current amplitudes of 0.7, 1, and 1.4 C. Additionally, cell capacity is measured using C/3 and C/15 currents. These tests support non-invasive diagnostic methods such as DVA and capacity difference analysis (CDA), detailed further in ref. [16–19].

The charge and discharge currents for each cell are specified in Figure 10c (321 kPa) and d (642 kPa). For instance, Cells 1–4 have the maximum charge current of 2 A, with the discharge currents of −1.13 A (yellow), −1.89 A (orange), −2.64 A (red), and −3.4 A (magenta). Cells 5–7 have the maximum discharge current of −3.4 A, with the charge currents 1.56 A (blue) 1.11 A (light blue), and 0.67 A (cyan). An identical setup is used for Cells 8–14, which are compressed to 642 kPa. The exact setup for each cell is shown in **Table 2**.

Acknowledgements

This research was funded by the Federal Ministry of Education and Research (BMBF) of Germany under grant no. 03XP0442. We also acknowledge the support of the Open Access Publication Fund of Technische Hochschule Ingolstadt (THI). Special thanks go to Cara Zimmermann for her valuable discussions, review, and support.

Open Access funding enabled and organized by Projekt DEAL.

Conflict of Interest

The authors declare no conflict of interest.

Author Contributions

Pablo Morales Torricos: conceptualization (lead); data curation (lead); formal analysis (lead); investigation (equal); methodology (lead); visualization (equal); writing—original draft (equal); and writing—review and editing (equal). **Andreas Gallenberger**: conceptualization (equal); data curation (equal); formal analysis (equal); investigation (equal); methodology (equal); visualization (equal); writing—original draft (equal); and writing—review and editing (equal). **Dominik Droese**: writing—review and editing (supporting). **Julia Kowal**: supervision (equal) and writing—review and editing (supporting). **Christian Endisch**: funding acquisition (lead); resources (lead); and validation (equal). **Meinert Lewerenz**: funding acquisition (equal); methodology (supporting); resources (equal); supervision (equal); validation (equal); writing—original draft (supporting); and writing—review and editing (supporting). **Pablo Morales Torricos** and **Andreas Gallenberger** contributed equally to this work.

Data Availability Statement

The data that support the findings of this study are available from the corresponding author upon reasonable request.

Keywords: accelerated aging · apparent aging · capacity recovery · electrolyte motion induced salt inhomogeneity · homogeneity of lithium distribution

[1] B. Epding, B. Rumberg, H. Jahnke, I. Stradtmann, A. Kwade, *J. Energy Storage* **2019**, *22*, 249.
[2] M. Lewerenz, P. Dechent, D. U. Sauer, *J. Energy Storage* **2019**, *21*, 680.
[3] F. B. Spingler, M. Naumann, A. Jossen, *J. Electrochem. Soc.* **2020**, *167*, 40526.
[4] P. M. Torricos, S. Berg, E. Figgemeier, C. Endisch, M. Lewerenz, *J. Energy Storage* **2025**, *131*, 117323.

[5] P. M. Torricos, C. Endisch, M. Lewerenz, *Batteries* **2023**, *9*, 230.
[6] S. Solchenbach, C. Tacconis, A. G. Martin, V. Peters, L. Wallisch, A. Stanke, J. Hofer, D. Renz, B. Lewerich, G. Bauer, M. Wichmann, D. Goldbach, A. Adam, M. Spielbauer, P. Lamp, J. Wandt, *Energy Environ. Sci.* **2024**, *17*, 7294.
[7] A. Bonakdarpour, I. Stoševski, A. Tiwari, S. R. Smith, B. M. Way, D. P. Wilkinson, *J. Electrochem. Soc.* **2024**, *171*, 20543.
[8] Y. Guo, P. Yu, C. Zhu, K. Zhao, L. Wang, K. Wang, *Int. J. Energy Res.* **2022**, *46*, 23730.
[9] M. Schreiber, T. Steiner, J. Kayl, B. Schönberger, C. Grosu, M. Lienkamp, *World Electr. Veh. J.* **2025**, *16*, 255.
[10] M. Schreiber, Y. Lin, A. Sommer, N. Wassiliadis, P. M. Torricos, M. L. m. Rogge, C. Grosu, C. Endisch, A. Jossen, M. Lienkamp, *J. Energy Storage* **2025**, *127*, 116924.
[11] T. Bond, S. Gasilov, R. Dressler, R. Petibon, S. Hy, J. R. Dahn, *J. Electrochem. Soc.* **2025**, *172*, 30512.
[12] C. P. Aiken, N. Kowalski, R. C. Fitzner, S. Trussler, J. E. Harlow, E. J. Butler, J. R. Dahn, *J. Electrochem. Soc.* **2023**, *170*, 40529.
[13] C. Zimmermann, C. Tacconis, S. Solchenbach, D. Goldbach, S. Erhard, J. Wandt, S. Lux, *J. Electrochem. Soc.* **2025**, *172*, 50528.
[14] A. Eddahech, O. Briat, J.-M. Vinassa, *Electrochim. Acta* **2013**, *114*, 750.
[15] F. B. Spingler, S. Kücher, R. Phillips, E. Moyassari, A. Jossen, *J. Electrochem. Soc.* **2021**, *168*, 40515.
[16] S. Dhillon, G. Hernández, N. P. Wagner, A. M. Svensson, D. Brandell, *Electrochim. Acta* **2021**, *377*, 138067.
[17] L. Ding, C. Zhang, T. Wu, F. Yang, Y. Cao, M. Xiang, *J. Power Sources* **2020**, *451*, 227819.
[18] A. Nyman, T. G. Zavalis, R. Elger, M. Behm, G. Lindbergh, *J. Electrochem. Soc.* **2010**, *157*, A1236.
[19] L. O. Valø/en, J. N. Reimers, *J. Electrochem. Soc.* **2005**, *152*, A882.
[20] J. P. Fath, L. Alsheimer, M. Storch, J. Stadler, J. Bandlow, S. Hahn, R. Riedel, T. Wetzel, *J. Energy Storage* **2020**, *29*, 101344.
[21] J. Landesfeind, H. A. Gasteiger, *J. Electrochem. Soc.* **2019**, *166*, A3079.
[22] C. Hogrefe, N. Paul, L. Boveleth, M. Bolsinger, M. Flügel, T. Danner, A. Latz, R. Gilles, V. Knoblauch, M. Wohlfahrt-Mehrens, M. Hölzle, T. Waldmann, *J. Electrochem. Soc.* **2024**, *171*, 70503.
[23] J. Sturm, A. Rheinfeld, I. Zilberman, F. B. Spingler, S. Kosch, F. Frie, A. Jossen, *J. Power Sources* **2019**, *412*, 204.
[24] F. Jiang, P. Peng, *Sci. Rep.* **2016**, *6*, 32639.
[25] Z. Chen, D. L. Danilov, R.-A. Eichel, P. H. L. Notten, *Adv. Energy Mater.* **2022**, *12*, 2201506.
[26] M. Alipour, C. Ziebert, F. V. Conte, R. Kizilel, *Batteries* **2020**, *6*, 35.
[27] M. Rogge, A. Jossen, *Batteries Supercaps* **2023**, *7*, e202300313.
[28] M. Lewerenz, G. Fuchs, L. Becker, D. U. Sauer, *J. Energy Storage* **2018**, *18*, 149.
[29] R. Burrell, A. Zulke, P. Keil, H. Hoster, *J. Electrochem. Soc.* **2020**, *167*, 130544.
[30] M. Lewerenz, C. Rahe, G. Fuchs, C. Endisch, D. U. Sauer, *J. Electrochem. Soc.* **2020**, *30*, 101529.
[31] Y. Preger, H. M. Barkholtz, A. Fresquez, D. L. Campbell, B. W. Juba, J. Romàn-Kustas, S. R. Ferreira, B. Chalamala, *J. Electrochem. Soc.* **2020**, *167*, 120532.
[32] S. F. Schuster, T. Bach, E. Fleder, J. Müller, M. Brand, G. Sextl, A. Jossen, *J. Energy Storage* **2015**, *1*, 44.
[33] J. Keil, N. Paul, V. Baran, P. Keil, R. Gilles, A. Jossen, *J. Electrochem. Soc.* **2019**, *166*, A3908.
[34] M. Lewerenz, D. U. Sauer, *J. Energy Storage* **2018**, *18*, 421.

Manuscript received: July 23, 2025
Revised manuscript received: September 26, 2025
Version of record online: